ACS Sustainable Chemistry & Engineering

Research Article

Cite This: ACS Sustainable Chem. Eng. 2020, 8, 814−822

pubs.acs.org/journal/ascecg

Comparative Study of Direct Compounding, Coupling Agent-Aided and Initiator-Aided Reactive Extrusion to Prepare Cellulose Nanocrystal/PHBV (CNC/PHBV) Nanocomposite

Ting Zheng,[†,‡] Craig M. Clemons,[†,§] and Srikanth Pilla*[,†,‡,∥,⊥]

[†]Department of Automotive Engineering, Clemson University, 4 Research Drive, Greenville, South Carolina 29607, United States

[‡]Clemson Composites Center, Clemson University, Greenville, South Carolina 29607, United States

[§]USDA Forest Service, Forest Products Laboratory, Madison, Wisconsin 53726, United States

[∥]Department of Mechanical Engineering, Clemson University, Clemson, South Carolina 29602, United States

[⊥]Department of Material Science and Engineering, Clemson University, Clemson, South Carolina 29602, United States

Supporting Information

ABSTRACT: Three compounding methods were compared to determine their effects on the organization of the interphase in nanocomposites of poly(3-hydroxybutyrate-*co*-3-hydroxyvalerate) (PHBV) and cellulose nanocrystals (CNCs) processed via (1) direct compounding, (2) reactive extrusion using a coupling agent (PHBV-*g*-GMA), or (3) reactive extrusion using a peroxide free-radical initiator (dicumyl peroxide, DCP). Tensile testing showed that only the peroxide-aided extrusion resulted in improvement in strength by 13%. Analyzing the interphases via DSC, WAXRD, SAXS, ATR-FTIR, and XPS helped relate the compounding methods to mechanical performance. Distinct PHBV−CNC graft configurations were found by analyzing CNCs isolated from each of the three composite types. Use of DCP led to polymer grafting, incomplete coverage of PHBV on the CNC surface, and many interpolymer cross-links. The result was robust matrix−CNC interfacial interaction and alignment of the CNCs, which yielded the best mechanical properties. Conversely, adding a coupling agent led to less actual PHBV grafts but greater coverage of the CNC surface relative to DCP-induced grafting. Although the CNCs were more dispersed, the lower PHBV grafting limited interfacial stress transfer and, consequently, reinforcement. While the direct compounding led to the less-dispersed CNC particles in the matrix with higher polymer coverage of flexible polymeric chain.

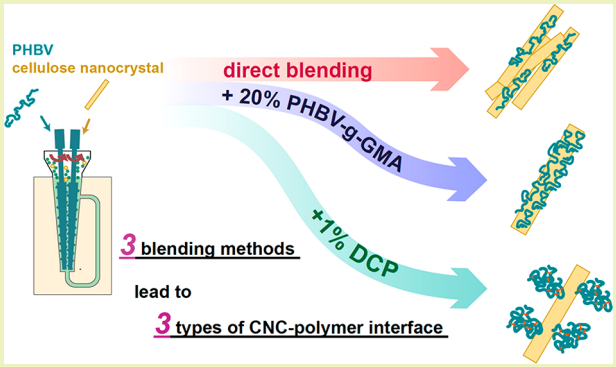

KEYWORDS: *CNC, PHBV, nanocomposite, reactive extrusion, interface*

INTRODUCTION

Driven by the growing public environmental awareness and increasingly stringent legislation, industry, and academia have great interest in developing high-performance biobased nanocomposites to alleviate the problems associated with petroleum-based plastics. One such strategy is to incorporate renewable fillers into plastics to reinforce them, reduce weight, and improve sustainability. Cellulose nanocrystals (CNCs) are a likely candidate because of their high stiffness, low density, and abundance.[1]

CNCs are extracted from bulk cellulosic materials, such as wood and agricultural crops.[2] Through chemical treatment, amorphous regions are preferentially hydrolyzed, leaving rod-like CNC of 100−300 nm in length and 5−10 nm in width,[3,4] with high crystallinity, modest aspect ratio, and abundant groups for subsequent modifications. Because of their unique chemical and physical properties, CNCs have great potential as a composite filler. However, CNCs' inherent hydrophilicity and strong aggregation tendencies are daunting challenges when blending them with hydrophobic commodity plastics.[5] On the lab-scale, such agglomeration can be mitigated by solvent blending or CNC surface modification.[6,7] Unfortunately, these methods are often time-consuming, expensive and, thus, lack industrial potential. However, these well-controlled lab studies suggest two determinative factors required for better composites properties: good CNC dispersion and effective CNC−matrix interfacial interaction.[8,9]

Because of these two requirements and in pursuit of the mass-process, CNC nanocomposites were manufactured via reactive extrusion to introduce covalent CNC−matrix interfacial adhesion. Two strategies were implemented: (1) The coupling agent (CA) method, which is relatively

Received: August 19, 2019
Revised: November 17, 2019
Published: December 16, 2019

DOI: 10.1021/acssuschemeng.9b04867
ACS Sustainable Chem. Eng. 2020, 8, 814−822

conventional and introduces a polymeric CA molecule bearing maleic anhydride (MA),[10] glycidyl methacrylate (GMA),[11,12] or other reactive group. Good interfacial adhesion relies on the formation of covalent bonds (e.g., ester or ether) between the functional groups of the CA and the −OH groups of the CNC. (2) Recently developed in situ grafting methods, which permit surface grafting via initiation and termination of polymer and cellulosic radicals during extrusion.[13−15] Both strategies are deemed to improve the composites properties by enhancing the CNC dispersion and the CNC−plastic interfacial adhesion. In a studyon CNC−polylactic acid (PLA) composites, the increase of 22% in tensile strength (σ) and 19% in Young's modulus (E) were reported after introducing the coupling agent (PLA-*g*-GMA),[11] while the increase by 22% (σ) and 180% (E) with the addition of 1% dicumyl peroxide (DCP) were documented in another study.[13]

Although, improvement in mechanical properties was observed, the underlying mechanisms are not as manifested as in studies using solvent casting. This is because the effects of the additives can be overshadowed by processing-related factors, such as the reduction in CNC dimensions,[16] anisotropic orientation,[17,18] and effects of temperature and shear on free-radical generation, viscosity, etc. Additionally, extrusion is inherently less flexible than lab-scale blending techniques, restricting the latitude to design a well-controlled experiment[16,19] and sometimes making conclusions ambiguous. Such uncertainty is manifested in the example of the dual-roles of DCP and the CA. DCP not only initiates CNC−polymer grafting[18] but also induces polymer−polymer cross-linking as well as β-scission in the bulk matrix.[12,15] Both can affect mechanical properties, but only the former is pertinent to CNC reinforcement. Likewise, blending a portion of CA into the matrix not only introduced covalent CNC−matrix bonding, but also enhanced the CNC dispersion owing to bringing in polarity moieties.[12] The closely coupled pathways make evaluating the factors (e.g., covalent bonding, dispersion) individually difficult. Although evidence supporting interfacial grafting (e.g., increased polymer molecular weight after CNC addition,[13] identification of cellulosic radical species[14] during extrusion) can sometimes be found, direct observation is rare and the characters of the grafted polymers on the CNC surface and correlation with composite properties remain unclear.

Consequently, in the present work, we probe the surface of CNCs in the composites to find more direct evidence of polymer grafting and help elucidate the mechanisms of CNC reinforcement. Two commonly used compatibilization strategies, CA-aided blending and in situ grafting, were investigated in a matrix of poly(3-hydroxybutyrate-hydroxyvalerate) (PHBV)—a bacterially derived linear polyester. The CNC−PHBV interfaces were characterized using DSC, WAXRD, SAXS, ATR-FTIR, and XPS after extracting any PHBV not anchored to the CNCs, to segment the CNC interface out of the matrix. The CNC surface coverage and quantity of the anchored PHBV were investigated as was its crystallization behavior and the configuration of grafted chains. In this study, the macroscopic composite mechanical properties and the microscopic filler−matrix interfacial conditions will be correlated and present insights into the reinforcing mechanism and provide guidance for fabricating high-performance CNC nanocomposites.

EXPERIMENTAL SECTION

Materials. PHBV pellets (ENMAT Y1000P, 8% HV content, injection molding grade, with <0.5% boron nitride as nucleating agent, and antioxidant Irganox 1010) was purchased from Tianan Biological Materials, Ltd., China. Also purchased was commercially available glycidyl methacrylate (GMA, Sigma) and dicumyl peroxide (DCP, 98%, Alfa Aesar). The CNC was prepared via sulfuric acid hydrolysis at the USDA Forest Products Laboratory in Madison, WI, in the length of 271 ± 47 nm and width of 6.17 ± 2.00 nm. CNC was freeze-dried prior to compounding.

Nanocomposite Processing. The coupling agent (CA) was GMA-*graft*-PHBV, which was prepared by reactive extrusion according to our previous report.[12] Briefly, DCP was first dissolved in GMA, and then, it was pumped into the extruder barrel to blend with the PHBV melt. The GMA grafting percentage, defined as the wt % of GMA of the CA, was quantified as 3.14% via standard titration.[12]

The PHBV/CNC nanocomposites were melt-processed on a 15 mL Xplore twin-screw microcompounder (DSM, Xplore Instrument) according to three compounding protocols: direct compounding, CA-aided reactive extrusion, and DCP-induced in situ grafting (Scheme S1). For direct compounding, the CNC powder was mixed with the PHBV pellets in a beaker prior to placement in the extruder hopper. For CA-assisted blending, a portion of CA pellets were mixed with CNC and PHBV in a beaker prior to melt extrusion. For in situ grafting, the DCP/acetone solution was sprayed on the PHBV pellets, followed by oven drying (50 °C for 4 h) prior to the extrusion with CNC. These three methods yielded three composites denoted as PHBV*x*CNC, PHBV*y*CA*x*CNC, and PHBV*z*DCP*x*CNC according to their individual composition, with *x*, *y*, *z* indicating the CNC wt % (*x* = 1, 3, 5), coupling agent wt % (*y* = 5, 10, and 20), and DCP wt % (*z* = 0.5, 1, and 2).

Prior to extrusion, the PHBV and CA pellets were vacuum-dried at 70 °C for 4 h to remove moisture. Barrel temperatures of the microextruder were 160−180−180 °C (feed zone, middle zone, die zone), the screw speed was 50 rpm and the materials were recirculated in the extruder for 5 min. Standard type-V tensile specimens (ASTM D638,[20] thickness = 1.12 mm) were injection molded using a DSM Xplore microinjection molding unit with a barrel temperature of 170 °C and a mold temperature of 60 °C. The injection pressure and holding pressure were both 5.5 bar, and the holding time was 15 s.

Mechanical Properties of Composites. The tensile properties of the injection molded type-V specimens were determined as per ASTM D638[20] using a Instron universal testing machine (Model 1125), which was equipped with a load cell of 50 N and using a cross-head speed of 1 mm/min with 7.62 mm initial grip separation.

Characterization of the Composite Structures and Properties. For the differential scanning calorimetry (DSC, Q20, TA Instruments), unless otherwise specified, each sample (∼5 mg) was subjected to a heating−cooling−heating cycle in N_2 from −50 to 200 °C at a rate of 10 °C/min. The melt temperatures (T_m) and the melting enthalpy (ΔH_m) were determined from the second heating scan, and the crystallization temperature (T_c) and enthalpy (ΔH_c) were determined from the cooling scan. The degree of the crystallinity (χ_c) was calculated by $\chi_c(\%) = \Delta H_m/\Delta H_m^0 \times 100/a$, where the ΔH_m^0 is the melting enthalpy for 100% crystalline PHBV, taken as 146 J/g,[21] and *a* is the weight fraction of the PHBV in the composites. A Xenocs GeniX3D microfocus source with 1.54 Å Cu Kα radiation was used for small-angle X-ray scattering (SAXS). The instrument was calibrated using 640c silicon powder with a peak position at 2θ = 28.44°, where 2θ is the total scattering angle. A Pilatus 300 K detector (Dectris) was used to collect 2D scattering patterns, which were then azimuthally integrated to 1D data of intensity (I) against scattering vector q. An X-ray flux of ∼21.4 M photons s^{-1} incident upon the sample was used to acquire SAXS data within 45 min measurement window of time.

CNC·PHBV Complex Isolation. The injection molded nanocomposites were subjected to a chloroform extraction to remove the unbonded PHBV from the CNC surface and to yield CNC·PHBV

DOI: 10.1021/acssuschemeng.9b04867
ACS Sustainable Chem. Eng. 2020, 8, 814−822

Table 1. Tensile Strength (σ), Young's Modulus (E), Strain at Break (ε) of the PHBV and PHBV−CNC Composites[a]

group	sample	σ (MPa)	E (MPa)	ε (%)
G1	PHBV	31.02 (0.60)^{a}	2142 (84)^{a}	1.85 (0.10)^{a}
	PHBV1CNC	31.05 (0.76)^{a}	2305 (85)^{b}	1.73 (0.07)^{ab}
	PHBV3CNC	30.93 (0.68)^{a}	2178 (96)^{a}	1.71 (0.11)^{b}
	PHBV5CNC	29.57 (1.22)^{b}	2427 (62)^{b}	1.55 (0.08)^{c}
G2	**PHBV(0CA)**	31.02 (0.60)^{a}	2142 (84)^{a}	1.85 (0.10)^{a}
	PHBV5CA	30.24 (0.58)^{a}	2194 (95)^{a}	1.69 (0.09)^{b}
	PHBV10CA	30.31 (0.42)^{a}	2165 (87)^{a}	1.73 (0.05)^{ab}
	PHBV20CA	30.41 (0.58)^{a}	2096 (35)^{a}	1.89 (0.10)^{a}
	CA	26.49 (0.78)^{b}	1781 (47)^{b}	2.25 (0.05)^{c}
G3	**PHBV(0CA)3CNC**	30.93 (0.68)^{a}	2178 (96)^{a}	1.71 (0.11)^{a}
	PHBV5CA3CNC	31.56 (0.38)^{a}	2174 (79)^{a}	1.79 (0.08)^{ab}
	PHBV10CA3CNC	31.23 (0.79)^{a}	2099(118)^{a}	1.88 (0.14)^{ab}
	PHBV20CA3CNC	30.53 (0.58)^{a}	2090 (61)^{a}	1.89 (0.15)^{b}
	CA3CNC	26.83 (0.77)^{b}	1745 (49)^{b}	2.40 (0.19)^{c}
G4	**PHBV20CA(0CNC)**	30.41 (0.58)^{ab}	2096 (35)^{a}	1.89 (0.10)^{ab}
	PHBV20CA1CNC	29.39 (0.56)^{a}	2036 (47)^{ab}	1.76 (0.10)^{b}
	PHBV20CA3CNC	30.53 (0.58)^{b}	2090 (61)^{a}	1.89 (0.15)^{ab}
	PHBV20CA5CNC	30.09 (0.82)^{ab}	2000 (51)^{b}	1.99 (0.09)^{a}
G5	**PHBV(0DCP)**	31.02 (0.60)^{a}	2142 (84)^{a}	1.85 (0.10)^{a}
	PHBV0.5DCP	33.47 (0.73)^{b}	1817 (61)^{b}	3.33 (0.21)^{b}
	PHBV1DCP	33.85 (0.76)^{b}	1714 (38)^{b}	3.98 (0.15)^{c}
	PHBV2DCP	32.14 (0.76)^{c}	1377 (73)^{c}	5.20 (0.42)^{d}
G6	**PHBV(0DCP)3CNC**	30.93 (0.68)^{a}	2178 (96)^{a}	1.71 (0.11)^{a}
	PHBV0.5DCP3CNC	33.63 (0.34)^{b}	2020 (60)^{b}	2.53 (0.13)^{b}
	PHBV1DCP3CNC	33.88 (0.94)^{b}	1786 (65)^{c}	3.49 (0.27)^{c}
	PHBV2DCP3CNC	32.24 (0.80)^{c}	1446 (64)^{d}	4.82 (0.35)^{d}
G7	**PHBV1DCP(0CNC)**	33.85 (0.76)^{a}	1714 (38)^{a}	3.98 (0.15)^{a}
	PHBV1DCP1CNC	35.05 (0.74)^{b}	1875 (53)^{b}	3.37 (0.14)^{b}
	PHBV1DCP3CNC	33.88 (0.94)^{a}	1786 (65)^{ab}	3.49 (0.27)^{b}
	PHBV1DCP5CNC	33.74 (0.60)^{a}	1819 (95)^{b}	3.46 (0.23)^{b}

[a]Values in parentheses are standard deviations. Statistics are conducted within each subgroup. Samples within a subgroup with different letters (a, b, c) following the parentheses are statistically significantly different ($p < 0.05$) using one-way ANOVA test followed by posthoc analyses for multiple comparisons by using Tukey's honest significant differences (HSD) test. Bolded rows are duplicated data for the clarity.

complexes in the form of powders. Specifically, a 5 g composite was dissolved in 30 mL of chloroform, followed by a 10 min reflux on a hot plate. The mixture was then centrifuged (Clinical 50, VWR, US) at 5k rpm for 5 min. The supernatant was decanted, and the precipitate resuspended in 30 mL of fresh chloroform. After 6 cycles, the precipitate was collected and vacuum-dried at 70 °C for 4 h before characterization. CNC·PHBV extracted from composites that were direct compounded, compounded with 20% CA, and compounded with 1% DCP were named complexes i (direct), ii (coupling), and iii (in situ) respectively, or i, ii, or iii for brevity. These CNC·PHBVs were characterized as detailed below.

CNC·PHBV Characterization. For the thermogravimetric analysis (TGA, Q5000, TA Instruments), samples (~4.0 mg) were analyzed from 25 to 800 °C at 10 °C/min in a N_2 flow. Attenuated total reflectance Fourier transform infrared spectroscopy (ATR-FTIR, Thermo-Nicolet Magna 550 FTIR spectrometer in combination with a Theremo-SpectracitraTech Foundation Series Diamond ATR accessory with a 50° angle of incidence) was used to determine the overall composition of i, ii, and iii after drying in a desiccator for 72 h. Spectra were collected in absorbance mode from 4000 to 400 cm^{-1} at a resolution of 2 cm^{-1}. Wide-angle X-ray diffraction (WAXRD) analysis was performed using a Rigaku Miniflex (The Woodlands, USA) diffractometer with Ni-filtered Cu Kα radiation (λ = 1.45 Å) at 45 kV and a current of 30 mA. Samples were scanned from 5° to 65° at a rate of 1°/min.[22] The CNC crystallinity index was evaluated using the equation $I_c = 1 - I_1/I_2$, where I_1 is the intensity at the amorphous background (2θ = 18°) and I_2 is the intensity associated with the crystalline region of cellulose ((002) plane at 2θ = 22.8°).[22,23] A VersaProbe III (Physical Electronics, USA) with a monochromatic Al X-ray source operating at 15 kV, 25 W, with a beam spot of ~100 μm in diameter was used for X-ray photoelectron spectroscopy (XPS).

RESULTS AND DISCUSSION

Mechanical Properties of Composites. Tensile strength (σ), modulus (E), and elongation at break (ε) were measured for different CNC levels as well as for neat PHBV containing various levels of a CA or DCP as controls. The samples were categorized into seven groups (G1−G7), and their tensile properties are summarized in Table 1. The tensile properties of the direct compound materials (G1) exhibit commonly observed trends of composites processed with untreated CNC and hydrophobic plastics: an increase in E and a decrease in ε with CNC addition, but little effect on σ except an eventual decrease at high loadings[24−26] caused of CNC agglomeration. To try and enhance CNC−PHBV adhesion and CNC dispersion, either a CA or DCP was compounded with PHBV and CNC. Adding various amounts of CA to either the neat PHBV or composites with 3% CNC (G2, G3) failed to yield substantial changes in the mechanical properties. Further, no significant reinforcement of the matrix was observed with 20% CA addition at any CNC level (G4). Though these results suggest inefficiency of the CA in promoting CNC reinforcement, an improvement in CNC dispersion was suggested as discussed below.

DOI: 10.1021/acssuschemeng.9b04867
ACS Sustainable Chem. Eng. 2020, 8, 814−822

However, the effect of adding DCP to neat PHBV was quite evident (G5). A 1% DCP addition increased the σ by 10% and the ε by 115%, both of which were probably the result of DCP-induced chain-extension and cross-linking (Scheme S2).[15] At a higher DCP dosage (e.g., 2%), voids were observed in the injection molded composites, leading to the reduction in E.[27] Varying the CNC content in the presence of 1% DCP did yield reinforcement at 1% CNC (G7), suggesting a DCP-induced coupling effect. This optimized composition (1% DCP with 1% CNC) led to an increase of 13.0% in σ and 12.5% in E with respect to neat PHBV. However, when compared to PHBV1DCP, the enhancements are less substantial suggesting that most of the increase is due to DCP cross-linking of the PHBV matrix. Such pronounced influence of matrix was also observed in the case of PLA/CNC blended with 1.2% DCP, where the matrix contributed half of the enhancement in σ and approximated 95% increase in E.[13]

Thermal Properties and Crystallization. Table 2 summarizes the composites' thermal properties and shows some of the effects of the compounding methods and CNC loading levels. Comparing to the unpredictable change in glass transition temperature (T_g,Table S1), within each group, the melting point (T_m) and the crystallization temperature (T_c) are insensitive to CNC loading level, which is in agreement with other studies.[12] The degree of crystallinity (χ_c) of PHBV20CA and PHBV1DCP are lower than the neat PHBV by 3% and 7% because of the chain irregularity introduced by either the branched CA molecule[12] or DCP-induced PHBV cross-linking (Scheme S2), respectively. Adding CNC is known to either increase[28] or decrease[29] the χ_c by either providing additional nucleating sites or restricting the chain diffusion and folding at the crystal growth front,[30] respectively. No matter which mechanism dominates, it is associated with the additional interfacial area created by the filler. In this study, the χ_c generally decreased with CNC content when processed with CA or DCP, suggesting increased interfacial area. In contrast, the composites without additives, showed little change in χ_c with addition of CNC, implying less interfacial surface, which is in agreement with our hypothesis that direct compounding leads to more agglomeration.

Table 2. Thermal Properties of PHBV and PHBV−CNC Composites

sample designation	T_m (°C)[a]	T_c (°C)[b]	χ_c (%)[c]
PHBV	171.1	117.7	69.5 (0.2)
PHBV1CNC	170.6	117.8	69.8 (0.1)
PHBV3CNC	171.0	117.7	70.1 (0.4)
PHBV5CNC	170.9	117.8	69.8 (0.4)
PHBV20CA(0CNC)	170.2	118.1	67.6 (0.1)
PHBV20CA1CNC	169.7	118.0	66.8 (0.1)
PHBV20CA3CNC	170.5	117.6	65.6 (0.2)
PHBV20CA5CNC	169.8	118.0	64.4 (0.2)
PHBV1DCP(0CNC)	166.1	122.6	64.6 (0.4)
PHBV1DCP1CNC	166.2	122.9	65.5 (0.4)
PHBV1DCP3CNC	166.7	121.3	58.3 (0.7)
PHBV1DCP5CNC	166.7	122.0	63.5 (0.1)

[a]Determined in the second DSC heating scan. Presented as the average of three runs. [b]Determined in the DSC cooling scan. Presented as the average of three runs. [c]Values in parentheses are standard deviations.

Analysis of CNC·PHBV Complexes. To closely examine the CNC−PHBV interfacial conditions, three CNC·PHBV complexes (i, ii, and iii) derived from the three processing protocols were isolated from corresponding composites via an exhaustive chloroform extraction. At a concentration of ~70 mg/mL in the chloroform, i (direct compounding) was yellow in color, while ii (CA addition) and iii (in situ) were white (Figure 1a). The CNC discoloration indicates thermal degradation at the elevated temperature during extrusion.[31] CNCs are known to be thermally sensitive and their degradation is catalyzed by the sulfate groups introduced by sulfuric acid hydrolysis during CNC production.[32] CNC's thermal degradation, usually characterized by either discoloration or thermogravimetric analysis (TGA), can be mitigated when sulfate groups are shielded through surface modification, for example, either by polymer physical adsorption[31] or polymer grafting.[32] In this study, correlation of the bond nature and CNC discoloration was evident: physical bonding resulted in yellowing of the CNC, while covalent bonding did not (Figure 1a). TGA results (Figure 1b), on the other hand, show enhanced thermal stability for all three complexes, exhibiting overlapped differential thermogravimetric (DTG) curves with the main degradation peaks shifting toward a higher temperature (from 256 for pristine CNC to 314 °C for all complexes). These results imply that grafting via covalent bonding is more effective than the physical deposition in mitigating the thermally induced CNC discoloration, but not mass loss. If this is the case, the enhanced thermal stability, suggested by DTG curves, may imply the existence of residual PHBV on all three complexes' surface.

Although the measure of an absolute quantity of PHBV graft is challenging, relative PHBV levels among the three CNC·PHBV is acquirable by comparing the area of the FITR

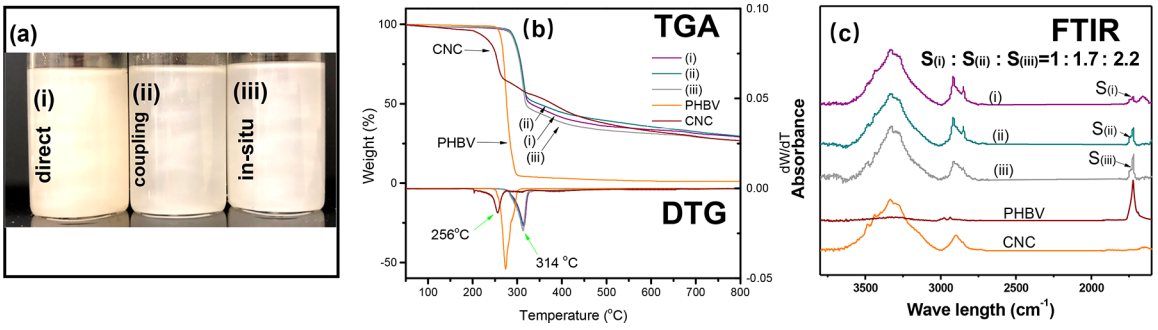

Figure 1. Characterizations of CNC·PHBV complexes and pristine CNC and PHBV: (a) suspension of i, ii, and iii in chloroform; (b) TGA and DTG curves; and (c) FTIR spectra.

DOI: 10.1021/acssuschemeng.9b04867
ACS Sustainable Chem. Eng. 2020, 8, 814−822

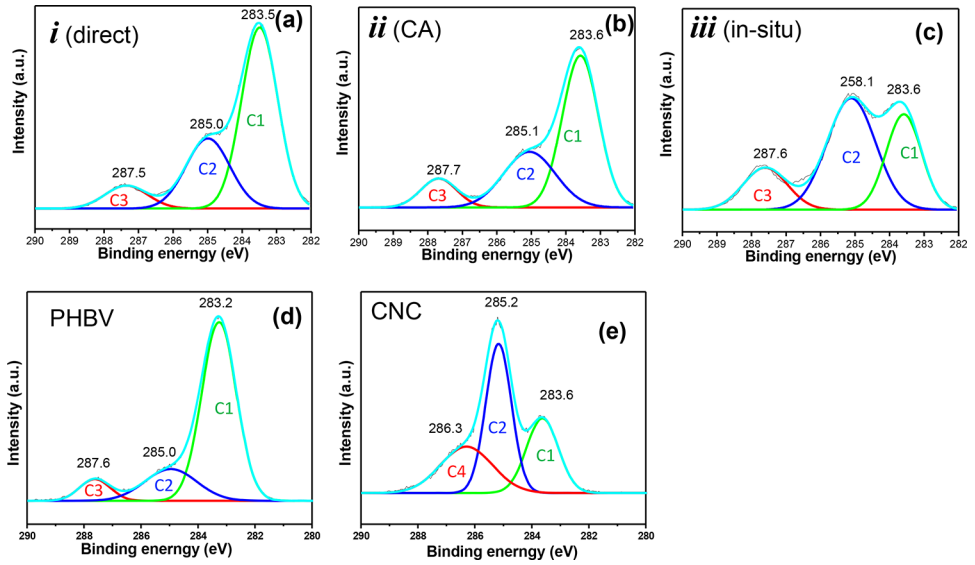

Figure 2. XPS high-resolution C 1s spectra of (a) PHBV·CNC complexes i, (b) ii, and (c) iii, neat PHBV (d), and pristine CNC (e).

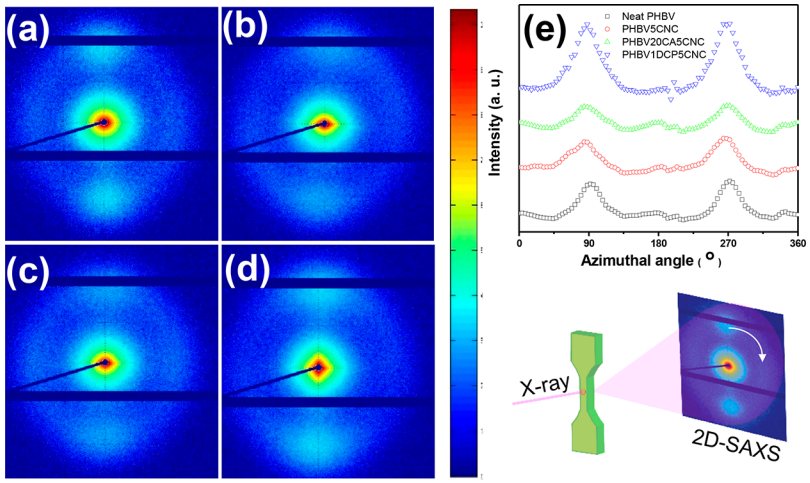

Figure 3. 2D SAXS pattern for the injection molded neat PHBV (a), PHBV5CNC (b), PHBV20CA5CNC (c), and PHBV1DCP5CNC (d). As-calculated Azimuthal angles (e).

spectrum band at ~1730 cm^{-1} (the PHBV carbonyl stretching) when the cellulose −OH bands (3400−3200 cm^{-1}) are normalized. The three integrated bands values are denoted as S_i, S_{ii}, and S_{iii}, accordingly (Figure 1c). This method was developed on the basis of an observed linear correlation between the band area (1730 cm^{-1}) and the wt % of polyester grafts of the CNC-*graft*-PCL synthesized via a ring-opening polymerization.[33] Unlike the 1730 cm^{-1} bands of CNC-*graft*-PCL in ref 32, band intensities in this study were much lower, implying a low graft content. This is in agreement with others that the "grafted to" strategy (used in this study) yields a lower graft density resulting from steric hindrance of adjacent grafts.[6]

The carbonyl signal (at ~1730 cm^{-1}) appears in all the three CNC·PHBV samples, confirming the existence of firmly anchored PHBV even after thorough extraction. For ii and iii, CNC−PHBV interactions could be covalent bonding, while for i, it could be physical interaction associated with the polar motifs of polyester (PHBV).[34]

The relative PHBV contents of S_i: S_{ii}: S_{iii} were 1: 1.7: 2.2. The low value of S_i was expected because of the weak physical interactions between CNC and PHBV developed during direct compounding. Comparison of the two covalently bonded samples showed that ii had less PHBV than iii ($S_{ii} < S_{iii}$). This can be interpreted as either a low grafting efficiency and/or greater steric hindrance from the larger CNC surface area coverage by each CA molecule because of multiple GMA groups on each PHBV chain. However, the possibly of insoluble cross-linked PHBV gel is unlikely, since it would be of lower density than chloroform and, therefore, decanted after centrifuging. Although the hypothesis regarding the chain conformation of grafts on the CNC surface appears likely, its validation is complicated by the difficulty of proving it morphologically. CNC·PHBV bundles did not completely disperse in the chloroform at ambient temperature (visible to the naked eye in Figure 1a) because of their partial hydrophilicity, thus preventing the use of TEM and dynamic light scattering to determine their dimensions.

Because of its capacity for surface characterization at thicknesses below 10 nm,[35] XPS was used to investigate coverage of the PHBV on the CNC. The XPS carbon 1s signal was deconvoluted into three peaks corresponding to the C−H or C−C at 284.8 eV (peak C1), C−O at 286.7 eV (peak C2),

DOI: 10.1021/acssuschemeng.9b04867
ACS Sustainable Chem. Eng. 2020, 8, 814−822

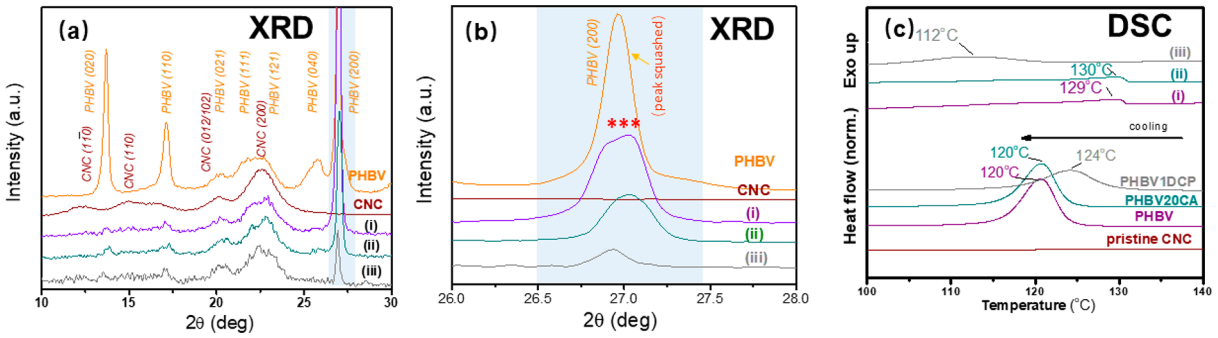

Figure 4. WAXRD spectra of the CNC·PHBV complexes i, ii, and iii, the pristine CNC, and the neat PHBV (a and b). DSC thermograms of complexes and the corresponding matrix (c).

and the O−C−O or C═O at 289.1 eV (C3), respectively (Figure 2). Since all cellulosic carbons contain a C−O bond, most of the C1 peak was from the alkane structure of PHBV (cf. Figure 2d and 3e). Therefore, the large relative intensity of the C1 for i and ii could result from greater PHBV coverage of the surface of the CNCs. Surprisingly, the C1 peak for iii was not large despite having the largest amount of PHBV, as indicated by the FTIR results. We speculate that the packing of PHBV grafts of iii occupied a smaller surface area on the CNCs, leaving more exposed CNC surface than with i and ii. Although i and ii had less PHBV overall than iii had, it was distributed over a larger fraction of the CNC surface, thus yielding a larger C1 signal. The lower sulfur atomic concentration in i and ii than in iii (S_{2p} at 169 eV, Figure S4 and Table S2) supports this hypothesis, suggesting less exposure of the CNC surface, which is sulfated during preparation by hydrolysis. However, the absence of further direct morphological evidence, for example, transmission electron microscopy or dynamic light scattering, prevents the evaluation of this hypothesis in its entirety.

An indirect method was then used to probe the packing state of the PHBV graft, based on the assumption that the polymer grafts exert influence on the CNC dispersion and orientation within the injection-molded specimen. The SAXS patterns of the narrow region of tensile specimen are shown in Figure 3a−d. The scattering patterns show a weak, broad meridional peak for the neat PHBV (Figure 3a), which is caused by the shear-induced polymer molecular orientation during injection molding.[36] A similar feature was also observed in all of the composite samples (Figure 3b−d), shielding the CNC signal to an extent. However, a spherical density in the core region evolve to ellipsoidal upon the addition of the CNC, showing a sharp and elongated equatorial peak believed associated with the elongated void parallel to the fiber wall and, thus, is a good indicator for the CNC orientation.[37]

The increased scattering intensity in the meridional peak is associated with the misorientation of the voids and the reduction of the voids length,[38] the crystalline lamellae created along the cellulose fiber,[37] or the "kebab" of the "shish-kebab structure",[36] with all of which related to the structures perpendicularly to axis of the fiber (and the flow direction). The intensity on the meridian peak is especially evident for in situ grafting (Figure 3d), indicating PHBV protrusion on the CNC surface. Azimuthal integration further reduced the 2-D SAXS to the 1D curve with the peak intensity as an indicator of the degree of orientation (Figure 3e).[39] Even considering the superimposing effect of the aligned PHBV molecule in the matrix (black square in Figure 3e), the composites derived via in situ grafting shows a pronounced high peak intensity, unlike the smaller peaks for direct and CA-assisted compounding. The larger and unevenly distributed shear force experienced by the CNC and the bulky PHBV protuberance that synergistically align the CNC fiber long the flow direction may be the cause of this intensity. Such findings partially support the assumption of the stacking of large quantities of PHBV that occupies a smaller region than in situ grafting.

The WAXRD results in Figure 4a and b elucidate the effects of processing methods on the crystal structure of PHBV. PHBV has an orthorhombic crystalline lattice with characteristic peaks at 2θ values of about 13.7°, 17.2°, 20.5°, 21.9°, 22.17°, 25.8°, and 27.0° corresponding to planes of 020, 110, 021, 111, 121, 040, and 200.[14] The CNC exhibited characteristic peaks at 14.5°, 16.6°, 20.4°, and 22.7°, corresponding to the 110, 110, 012/102, and 200 crystal planes of cellulose I (i.e., native cellulose).[40] The CNC crystallinity indices (CI_a where a is sample name) are 82.9% for pristine CNC, and 74.2, 76.0, and 67.0% for i, ii, and iii, respectively. The reduction of CI is an indicator of the loss of original CNC structure, reflecting the harshness of the surface modification. Here, CI_{iii} is much lower than the other two, suggesting the occurrence of in situ grafting in the crystalline regions, that damages the CNC crystalline structure.[14] A similar notable reduction in CI has been observed for cellulose fibers and PHB composites and it is closely related to the extrusion time and graft efficiency.[14] Whereas CI_{ii} is close to CI_i, indicating that the coupling agents (PHBV-*g*-GMA) exert a lesser influence on the CNC structure. The PHBV peaks are found in all three complexes, further confirming the presence of PHBV. The effects of the compounding approach on PHBV crystallization can be seen by examining the large PHBV (200) peak, a preferential growth direction of crystallites associated with the injection molding[41] (see Figure 4b and for details see Figure S3). This peak is largest in i, followed by ii and iii, indicating that PHBV chains on i are more flexible in terms of folding and crystallizing regardless of having the least PHBV. Complex iii has the most PHBV and yields the lowest intensity (200) peak, probably due to either polymer−polymer cross-linking within the grafted polymer pendent or polymer−CNC bonding at the interface restricting PHBV crystallization.

The DSC thermograms of i, ii, and iii, with pristine CNC and neat PHBV as a reference are shown in Figure 4c. Although precisely determining the PHBV mass of complexes is challenging and prevents quantifying the degree of crystallinity (χ_c) of PHBV grafts, the crystallization temperatures (T_c) on the DSC curves provides insight into the crystallization behavior. Although small and broad, the peaks in

DOI: 10.1021/acssuschemeng.9b04867
ACS Sustainable Chem. Eng. 2020, 8, 814−822

the cooling curves for the complexes (top 3 curves) display characteristics of a T_c peak, shifting to higher temperature at low cooling rate unlike the melting peak, T_m, which was relatively stationary (Figure S1), and thus, ascertained as T_c of the grafted PHBV in the complexes. The PHBV polymer chains on iii's surface has a notably lower T_c (112 °C) than those the polymer of corresponding matrix (PHBV1DCP, T_c = 124 °C), implying reduced PHBV crystallization kinetics on the CNC surface than the original PHBV. Both PHBV−PHBV cross-linking and CNC−PHBV grafting hinder chain mobility and, consequently, crystallization. However, polymer grafts of i and ii have a similar T_c's (129−130 °C), which are greater than their corresponding matrices alone (i.e., neat PHBV and PHBV20CA, both $T_c \approx 120$ °C). Crystallization was promoted by heterogeneous nucleation with CNC with less restriction in chain mobility caused by interfacial anchoring or polymer−polymer cross-linking as in iii.

On the basis of our examination of the polymer loading, crystallinity, surface coverage, and molecular orientation effects in the complexes, three imaginary CNC−PHBV architectures were proposed in Figure 5.

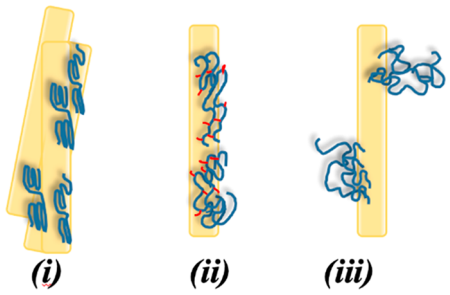

Figure 5. Imaginary schematic of the PHBV configurations on CNC surface created by direct compounding (i), coupling agent-aided extrusion (ii), and initiator-aided extrusion (iii).

This developed knowledge of the CNC−PHBV interfaces helps in understanding how they relate to mechanical performance. The introduction of covalent bonding did not necessary lead to CNC reinforcement. In the case of the CA method, the CA compatibilized the CNC and the matrix, resulting in enhanced CNC dispersion and some wetting and bonding of PHBV on the CNC surface, but the expected reinforcement was absent (Table 1). The similar results were also observed in PHBV/CNC blends created by solvent casting.[12] This is reminiscent of some noncovalently bonded additives such as poly(ethylene-*co*-poly(vinyl alcohol))[42] and poly(ethylene oxide)[43] or ionic interaction-based modifiers (e.g., imidazolium capped poly(lactic acid)[44] and hexadecyl trimethylammonium bromide[45]) and their effects on CNC−polymer blending. These additives feature weak interfacial interaction with CNCs. Likewise, we speculate that the CA-induced covalent linkage is too sparse or weak to form effective interfacial adhesion. The GMA moiety is more likely increasing the PHBV's polarity than introducing effective covalent bonding. As a result, CNC dispersion was enhanced without reinforcement. On the contrary, the in situ grafting method enhanced both the CNC dispersion and led to improved mechanical performance, some of which is possibly the result of reinforcement. In a similar reactive extrusion study using PHBV/cellulose fiber, the strong interfacial bonding was demonstrated by SEM images showing a continuous interface, while its direct compounding counterparts showed discrete interface and the fibers were pulled out from the matrix using microtome.[23] It was conjectured that the same situation occurred in the case of PHBV/CNC in this study but cannot be observed due to the small dimension of CNC. In addition, the more pendant-like grafted PHBV may enhance the chain entanglement with the bulk polymer or graft with it and facilitate PHBV−CNC stress-transfer.

CONCLUSIONS

A comparative study provides additional perspective to study phenomenon, allowing subtle differences to be elucidated through juxtaposition. This is well-demonstrated in this study through the characterization of three types of PHBV/CNC nanocomposites. Identical processing parameters helped isolate the effects of additives, a PHBV-GMA coupling agent and a DCP free radical initiator, on the properties of the final composites. The CNC reinforcement only occurred during in situ grafting, although CNC dispersion was promoted in both of the compatibilization methods as indicated by the crystallization behavior. In addition, the two criteria regarding CNC thermal stability, discoloration and mass loss, were not synchronous. Although the physical and covalent polymer shielding retarded mass loss of CNC, the original CNC color was preserved only through covalent chemistry. ATR-FTIR and XRD spectrum suggested the presence of bonded PHBV in all three composites after extraction in chloroform and each of the resulting CNC−PHBV complexes had distinct character. Sparse PHBV was found on the surface of CNC processed by direct compounding and the coupling agent method. These polymer chains remain relatively flexible with pronounced crystallization behavior, especially for the direct compounded composite. Though there was less residual PHBV than that of the in situ grafted composite, the PHBV covered more of the CNC surface as revealed by the XPS surface analysis. However, for the composites processed through in situ grafting, a more pendant-like PHBV morphology was suggested. Such graft conformation is likely related to the superior mechanical properties of its composites enabling efficient chain entanglement and interfacial adhesion at the interface.

Although different approaches were compared and contracted, further conclusions were limited by the absence of (1) an explicit mechanism for the correlation between covalent bonding and suppressed discoloration, (2) causality of the low coverage of PHBV on the CNC by in situ grafting, (3) direct morphological (or other) evidence to support our conjectures regarding PHBV coverage, and (4) direct evidence regarding our conjectures on the level of CNC dispersion by different processing methods. In addition, the characterization of the interfacial condition under deformation was not successful though it is quite relevant to the aim of this study. These methods include analyzing the adhesion factor[46] and the microstructure of voids.[47] However, further studies are expected to elucidate these gaps.

ASSOCIATED CONTENT

Supporting Information

The Supporting Information is available free of charge at https://pubs.acs.org/doi/10.1021/acssuschemeng.9b04867.

Schematic outline of the study, proposed reactions, a TEM of pristine CNC, composites' T_g data with a brief discussion, a thermogram with successive heating and

DOI: 10.1021/acssuschemeng.9b04867
ACS Sustainable Chem. Eng. 2020, 8, 814−822

cooling at different rates, additional XRD patterns for the composites, and XPS spectra of the complexes and the atomic concentration of those complexes (PDF)

AUTHOR INFORMATION

Corresponding Author

*E-mail: spilla@clemson.edu.

ORCID

Ting Zheng: 0000-0002-4115-4626

Srikanth Pilla: 0000-0003-3728-6578

Notes

The authors declare no competing financial interest.

ACKNOWLEDGMENTS

The authors would like to acknowledge the financial support by the USDA National Institute of Food and Agriculture, AFRI project [contract 2016-67021-25016], US Endowment for Forestry and Communities [grant number E17-18], Robert Patrick Jenkins Professorship, and Dean's Faculty Fellow Professorship. T.Z. would like to acknowledge partial financial support provided by Cooper-Standard Postdoctoral Fellowship.

REFERENCES

(1) Lee, K.-Y.; Aitomaki, Y.; Berglund, L. A.; Oksman, K.; Bismarck, A. On the use of nanocellulose as reinforcement in polymer matrix composites. *Compos. Sci. Technol.* **2014**, *105*, 15−27.

(2) Xie, H.; Du, H.; Yang, X.; Si, C. Recent strategies in preparation of cellulose nanocrystals and cellulose nanofibrils derived from raw cellulose materials. *Int. J. Polym. Sci.* **2018**, *2018*, 1−25.

(3) Camarero Espinosa, S.; Kuhnt, T.; Foster, E. J.; Weder, C. Isolation of thermally stable cellulose nanocrystals by phosphoric acid hydrolysis. *Biomacromolecules* **2013**, *14* (4), 1223−1230.

(4) Habibi, Y.; Lucia, L. A.; Rojas, O. J. Cellulose nanocrystals: chemistry, self-assembly, and applications. *Chem. Rev.* **2010**, *110* (6), 3479−3500.

(5) Ferreira, F.; Dufresne, A.; Pinheiro, I.; Souza, D.; Gouveia, R.; Mei, L.; Lona, L. How do cellulose nanocrystals affect the overall properties of biodegradable polymer nanocomposites: a comprehensive review. *Eur. Polym. J.* **2018**, *108*, 274−285.

(6) Roy, D.; Semsarilar, M.; Guthrie, J. T.; Perrier, S. Cellulose modification by polymer grafting: a review. *Chem. Soc. Rev.* **2009**, *38* (7), 2046−2064.

(7) Du, H.; Liu, C.; Zhang, M.; Kong, Q.; Li, B.; Xian, M. Preparation and industrialization status of nanocellulose. *Progress in Chemistry* **2018**, *30* (4), 448−462.

(8) Girouard, N. M.; Xu, S.; Schueneman, G. T.; Shofner, M. L.; Meredith, J. C. Site-selective modification of cellulose nanocrystals with isophorone diisocyanate and formation of polyurethane-CNC composites. *ACS Appl. Mater. Interfaces* **2016**, *8* (2), 1458−1467.

(9) Boujemaoui, A.; Mazieres, S.; Malmstrom, E.; Destarac, M.; Carlmark, A. SI-RAFT/MADIX polymerization of vinyl acetate on cellulose nanocrystals for nanocomposite applications. *Polymer* **2016**, *99*, 240−249.

(10) Kashani Rahimi, S.; Aeinehvand, R.; Kim, K.; Otaigbe, J. U. Structure and biocompatibility of bioabsorbable nanocomposites of aliphatic-aromatic copolyester and cellulose nanocrystals. *Biomacromolecules* **2017**, *18* (7), 2179−2194.

(11) Yang, W.; Dominici, F.; Fortunati, E.; Kenny, J. M.; Puglia, D. Melt free radical grafting of glycidyl methacrylate (GMA) onto fully biodegradable poly (lactic) acid films: Effect of cellulose nanocrystals and a masterbatch process. *RSC Adv.* **2015**, *5* (41), 32350−32357.

(12) Zheng, T.; Zhang, Z.; Shukla, S.; Agnihotri, S.; Clemons, C. M.; Pilla, S. PHBV-graft-GMA via reactive extrusion and its use in PHBV/nanocellulose crystal composites. *Carbohydr. Polym.* **2019**, *205*, 27−34.

(13) Dhar, P.; Tarafder, D.; Kumar, A.; Katiyar, V. Thermally recyclable polylactic acid/cellulose nanocrystal films through reactive extrusion process. *Polymer* **2016**, *87*, 268−282.

(14) Wei, L.; McDonald, A. G.; Stark, N. M. Grafting of bacterial polyhydroxybutyrate (PHB) onto cellulose via in situ reactive extrusion with dicumyl peroxide. *Biomacromolecules* **2015**, *16* (3), 1040−1049.

(15) Wei, L.; McDonald, A. G. Peroxide induced cross-linking by reactive melt processing of two biopolyesters: Poly (3-hydroxybutyrate) and poly (l-lactic acid) to improve their melting processability. *J. Appl. Polym. Sci.* **2015**, *132* (13), 41724.

(16) Alloin, F.; D'Aprea, A.; Dufresne, A.; El Kissi, N.; Bossard, F. Poly (oxyethylene) and ramie whiskers based nanocomposites: influence of processing: extrusion and casting/evaporation. *Cellulose* **2011**, *18* (4), 957−973.

(17) Fallon, J.; Kolb, B.; Herwig, C.; Foster, E.; Bortner, M. Mechanically adaptive thermoplastic polyurethane/cellulose nanocrystal composites: Process-driven structure−property relationships. *J. Appl. Polym. Sci.* **2019**, *136* (1−8), 46992.

(18) Rusli, R.; Shanmuganathan, K.; Rowan, S. J.; Weder, C.; Eichhorn, S. J. Stress-transfer in anisotropic and environmentally adaptive cellulose whisker nanocomposites. *Biomacromolecules* **2010**, *11* (3), 762−768.

(19) Bagheriasl, D.; Carreau, P.; Dubois, C.; Riedl, B. Properties of polypropylene and polypropylene/poly (ethylene-co-vinyl alcohol) blend/CNC nanocomposites. *Compos. Sci. Technol.* **2015**, *117*, 357−363.

(20) *Standard Test Method for Tensile Properties of Plastics*, ASTM D638-14; ASTM International: West Conshohocken, PA, 2014; www.astm.org.

(21) Luo, S.; Cao, J.; McDonald, A. G. Interfacial improvements in a green biopolymer alloy of poly (3-hydroxybutyrate-co-3-hydroxyvalerate) and lignin via in situ reactive extrusion. *ACS Sustainable Chem. Eng.* **2016**, *4* (6), 3465−3476.

(22) Segal, L.; Creely, J.; Martin, A., Jr; Conrad, C. An empirical method for estimating the degree of crystallinity of native cellulose using the X-ray diffractometer. *Text. Res. J.* **1959**, *29* (10), 786−794.

(23) Wei, L.; Stark, N. M.; McDonald, A. G. Interfacial improvements in biocomposites based on poly (3-hydroxybutyrate) and poly (3-hydroxybutyrate-co-3-hydroxyvalerate) bioplastics reinforced and grafted with α-cellulose fibers. *Green Chem.* **2015**, *17* (10), 4800−4814.

(24) Boujemaoui, A.; Cobo Sanchez, C.; Engstrom, J.; Bruce, C.; Fogelstrom, L.; Carlmark, A.; Malmstrom, E. Polycaprolactone Nanocomposites Reinforced with Cellulose Nanocrystals Surface-Modified via Covalent Grafting or Physisorption: A Comparative Study. *ACS Appl. Mater. Interfaces* **2017**, *9* (40), 35305−35318.

(25) Jun, D.; Guomin, Z.; Mingzhu, P.; Leilei, Z.; Dagang, L.; Rui, Z. Crystallization and mechanical properties of reinforced PHBV composites using melt compounding: Effect of CNCs and CNFs. *Carbohydr. Polym.* **2017**, *168*, 255−262.

(26) Yu, H.-Y.; Yao, J.-M. Reinforcing properties of bacterial polyester with different cellulose nanocrystals via modulating hydrogen bonds. *Compos. Sci. Technol.* **2016**, *136*, 53−60.

(27) Mi, H.-Y.; Jing, X.; Peng, J.; Salick, M. R.; Peng, X.-F.; Turng, L.-S. Poly (ε-caprolactone)(PCL)/cellulose nano-crystal (CNC) nanocomposites and foams. *Cellulose* **2014**, *21* (4), 2727−2741.

(28) Pei, A.; Zhou, Q.; Berglund, L. A. Functionalized cellulose nanocrystals as biobased nucleation agents in poly(l-lactide) (PLLA) − Crystallization and mechanical property effects. *Compos. Sci. Technol.* **2010**, *70* (5), 815−821.

(29) Pracella, M.; Haque, M. M.-U.; Puglia, D. Morphology and properties tuning of PLA/cellulose nanocrystals bio-nanocomposites by means of reactive functionalization and blending with PVAc. *Polymer* **2014**, *55* (16), 3720−3728.

(30) Xu, X.; Liu, F.; Jiang, L.; Zhu, J.; Haagenson, D.; Wiesenborn, D. P. Cellulose nanocrystals vs. cellulose nanofibrils: a comparative

DOI: 10.1021/acssuschemeng.9b04867
ACS Sustainable Chem. Eng. 2020, 8, 814−822

study on their microstructures and effects as polymer reinforcing agents. *ACS Appl. Mater. Interfaces* **2013**, *5* (8), 2999−3009.
(31) Ben Azouz, K.; Ramires, E. C.; Van den Fonteyne, W.; El Kissi, N.; Dufresne, A. Simple method for the melt extrusion of a cellulose nanocrystal reinforced hydrophobic polymer. *ACS Macro Lett.* **2012**, *1* (1), 236−240.
(32) Roman, M.; Winter, W. T. Effect of sulfate groups from sulfuric acid hydrolysis on the thermal degradation behavior of bacterial cellulose. *Biomacromolecules* **2004**, *5* (5), 1671−1677.
(33) Lonnberg, H.; Larsson, K.; Lindstrom, T.; Hult, A.; Malmstrom, E. Synthesis of polycaprolactone-grafted microfibrillated cellulose for use in novel bionanocomposites−influence of the graft length on the mechanical properties. *ACS Appl. Mater. Interfaces* **2011**, *3* (5), 1426−1433.
(34) Nicharat, A.; Sapkota, J.; Weder, C.; Foster, E. J. Melt processing of polyamide 12 and cellulose nanocrystals nanocomposites. *J. Appl. Polym. Sci.* **2015**, *132* (45), 42752.
(35) Cranston, E. D.; Gray, D. G. Morphological and optical characterization of polyelectrolyte multilayers incorporating nanocrystalline cellulose. *Biomacromolecules* **2006**, *7* (9), 2522−2530.
(36) Mi, D.; Xia, C.; Jin, M.; Wang, F.; Shen, K.; Zhang, J. Quantification of the effect of shish-kebab structure on the mechanical properties of polypropylene samples by controlling shear layer thickness. *Macromolecules* **2016**, *49* (12), 4571−4578.
(37) Wang, W.; Li, F.; Yu, J.; Navard, P.; Budtova, T. Structure and properties of novel cellulose-based fibers spun from aqueous NaOH solvent under various drawing conditions. *Cellulose* **2015**, *22* (2), 1333−1345.
(38) Chen, X.; Burger, C.; Fang, D.; Ruan, D.; Zhang, L.; Hsiao, B. S.; Chu, B. X-ray studies of regenerated cellulose fibers wet spun from cotton linter pulp in NaOH/thiourea aqueous solutions. *Polymer* **2006**, *47* (8), 2839−2848.
(39) Ying, Z.; Wu, D.; Wang, Z.; Xie, W.; Qiu, Y.; Wei, X. Rheological and mechanical properties of polylactide nanocomposites reinforced with the cellulose nanofibers with various surface treatments. *Cellulose* **2018**, *25* (7), 3955−3971.
(40) Wada, M.; Sugiyama, J.; Okano, T. Native celluloses on the basis of two crystalline phase (Iα/Iβ) system. *J. Appl. Polym. Sci.* **1993**, *49* (8), 1491−1496.
(41) Lai, M.; Li, J.; Yang, J.; Liu, J.; Tong, X.; Cheng, H. The morphology and thermal properties of multi-walled carbon nanotube and poly (hydroxybutyrate-co-hydroxyvalerate) composite. *Polym. Int.* **2004**, *53* (10), 1479−1484.
(42) Bagheriasl, D.; Carreau, P. J.; Dubois, C.; Riedl, B. Properties of polypropylene and polypropylene/poly(ethylene-co-vinyl alcohol) blend/CNC nanocomposites. *Compos. Sci. Technol.* **2015**, *117*, 357−363.
(43) Arias, A.; Heuzey, M.-C.; Huneault, M. A.; Ausias, G.; Bendahou, A. Enhanced dispersion of cellulose nanocrystals in melt-processed polylactide-based nanocomposites. *Cellulose* **2015**, *22* (1), 483−498.
(44) Mariano, M.; Pilate, F.; de Oliveira, F. B.; Khelifa, F.; Dubois, P.; Raquez, J.-M.; Dufresne, A. Preparation of Cellulose Nanocrystal-Reinforced Poly(lactic acid) Nanocomposites through Noncovalent Modification with PLLA-Based Surfactants. *ACS Omega* **2017**, *2* (6), 2678−2688.
(45) Nagalakshmaiah, M.; El Kissi, N.; Dufresne, A. Ionic compatibilization of cellulose nanocrystals with quaternary ammonium salt and their melt extrusion with polypropylene. *ACS Appl. Mater. Interfaces* **2016**, *8* (13), 8755−8764.
(46) Wang, X.; Sotoudehniakarani, F.; Yu, Z.; Morrell, J. J.; Cappellazzi, J.; McDonald, A. G. Evaluation of corrugated cardboard biochar as reinforcing fiber on properties, biodegradability and weatherability of wood-plastic composites. *Polym. Degrad. Stab.* **2019**, *168*, 108955.
(47) Muiruri, J. K.; Liu, S.; Yeo, J. C. C.; Koh, J. J.; Kong, J.; Thitsartarn, W.; Teo, W. S.; He, C. Synergistic Toughening of Poly (lactic acid)−Cellulose Nanocrystal Composites through Cooperative Effect of Cavitation and Crazing Deformation Mechanisms. *ACS Applied Polymer Materials* **2019**, *1* (3), 509−518.

DOI: 10.1021/acssuschemeng.9b04867
ACS Sustainable Chem. Eng. 2020, 8, 814−822